COBEM 2021 26th International Congress of Mechanical Engineering
November 22-26, 2021, Virtual Congress, Brazil

COB-2021-0857
EFFECT OF THE INCLINATION ANGLE ON THE PERFORMANCE OF 100 AND 30 MESH SCREEN COPPER WATER HEAT PIPES FOR APPLICATION IN A STIRLING ENGINE

Ana Carolina dos Santos
Instituto Tecnológico de Aeronáutica – ITA
Praça Marechal Eduardo Gomes, 50, 12228-900 Vila das Acacias, SP, Brazil
anna.carolsantos21@gmail.com

Lamartine Nogueira Frutuoso Guimarães
Instituto de Estudos Avançados – IEAv, Divisão de Energia Nuclear
Instituto Tecnológico de Aeronáutica – ITA-PGCTE
Trevo Coronel Aviador José Alberto Albano do Amarante, 01, 12228-001, São José dos Campos, SP, Brazil
lamar.guima@gmail.com

Valéria Serrano Faillace Oliveira Leite
Instituto de Estudos Avançados – IEAv, Divisão de Suporte Tecnológico
Trevo Coronel Aviador José Alberto Albano do Amarante, 01, 12228-001, São José dos Campos, SP, Brazil
valeria@ieav.cta.br

Rafael Theodoro
Instituto Tecnológico de Aeronáutica – ITA
Praça Marechal Eduardo Gomes, 50, 12228-900 Vila das Acacias, SP, Brazil
rafael_theodor@hotmail.com

Abstract. *This paper presents an experimental study of two screen copper-water heat pipes for application with the Stirling engine. The pipes have different porosities (30 and 100 mesh). These heat pipes will be used to transport heat from a thermal source to the hot end of a Stirling engine. However, first, it is necessary to understand the thermal behavior of the heat pipes. Thus, the objective is to analyze the temperature distribution and the influence of inclination on the thermal performance of heat pipes and choose the most suited one. For that, the temperatures were collected in the angulations: 0°, 30°, 45°, 60°, and 90°. Then, the characterization and selection of the best pipe were carried out. The results showed that at all angles of inclination, the condenser reached the temperature required to start the Stirling engine (greater than 215ºC and evaporator reached 270ºC). The angle variation has little influence on the performance of the heat pipes. However, at 90° temperature differential was lower. The 100 mesh showed better performance (smaller temperature difference and greater transport capacity). So, it was possible to select the 100 mesh heat pipe for application with the Stirling engine in the study.*

Keywords: *Heat Pipe, Screen Wick, two-phase flow, heat transfer, experimental analysis.*

1. INTRODUCTION

Heat pipes are passive and biphasic devices that quickly transport large amounts of heat with the minimum drop in temperature. Figure 1 shows a heat pipe, which is composed of a sealed hollow pipe, a wick (capillary structure) inside the pipe, and a working fluid. The length of the heat pipe is divided into three sections: evaporator, adiabatic, and condenser.

The heat applied to the evaporator section by an external source is conducted through the wall of the pipe and the capillary structure, causing the working fluid to vaporize (from liquid to vapor) (Reay et al., 2006). The increase in vapor pressure causes the vapor to leave the evaporator to the condenser, passing through the adiabatic region, carrying the latent heat of vaporization. In the condenser, the vapor releases its latent heat by condensing. The condensed liquid returns to the evaporator through the capillary structure of the wick, by capillary pressure action (heat pipe) or by gravity action (thermosyphon). The pressure inside the heat pipe is equal to the saturation pressure of the working fluid at the operating temperature. The phase change and the biphasic flow circulation continue as long as the temperature gradient between the evaporator and the condenser is maintained (Zohuri et al., 2016).

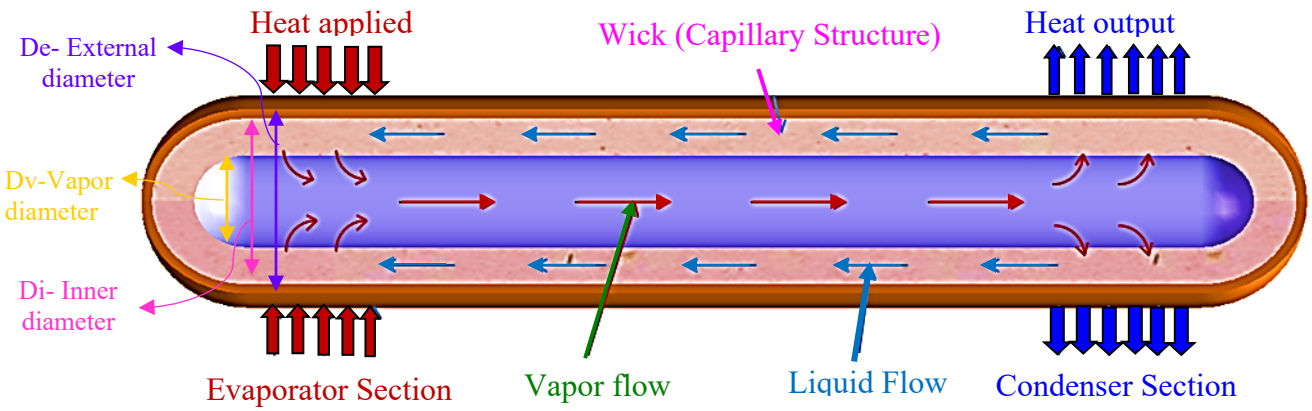

Figure 1. Schematic drawing of a heat pipe and its components (Zohuri et al., 2016).

Many mechanisms are capable of limiting the heat transport of a heat pipe. The main limitations are operational limits (viscous, sonic, entrainment, boiling, and capillary) and fluid volume. In the viscous limit, viscous forces prevent the vapor flow in the pipe. The limit occurs when the operating temperature is below the recommended temperature. At the Sonic limit, the vapor flow reaches sonic speeds as it leaves the evaporator. This results in a large temperature gradient. The sonic limit occurs when too much energy is applied to the evaporator at a low operating temperature. This is usually just a problem at startup.

At the entrainment limit, the vapor flow at high speed prevents the condensate from returning to the evaporator. Thus, drying of the fluid inside the pipe may occur. It occurs when the operating temperature is above the projected temperature or at a low operating temperature. The Boiling limit occurs when the heat flow in the evaporator is too high generating bubbles. This causes a block in the return of the liquid. In addition, it causes a very high-temperature rise and catastrophic drying can occur. The capillary limit is responsible for the effective pumping of the heat pipes by the capillary action. The capillary action of the wick structure cannot overcome the gravitational pressure, liquid, and vapor drop. This limit is reached when the power input is too high. It also occurs when the structure of the Wick was not properly designed for power and inclination.

The fluid volume filled is the relationship between fluid volume and evaporator volume. An insufficient amount of fluid causes dryness. Considering that an excessive amount of fluid combined with high heat flow causes the boiling limit. The experiments carried out by Nemec (2016) showed that the ideal amount of working fluid is in the range of 10-30% of the total volume of the heat pipe.

The main application of these devices is in the cooling of electronic components, such as notebooks (Fig. 2-A). However, there are few experimental works in the Space sector for the thermal control of spacecraft, satellites, hypersonic vehicles (Fig. 2-B), and thermal energy conversion systems.

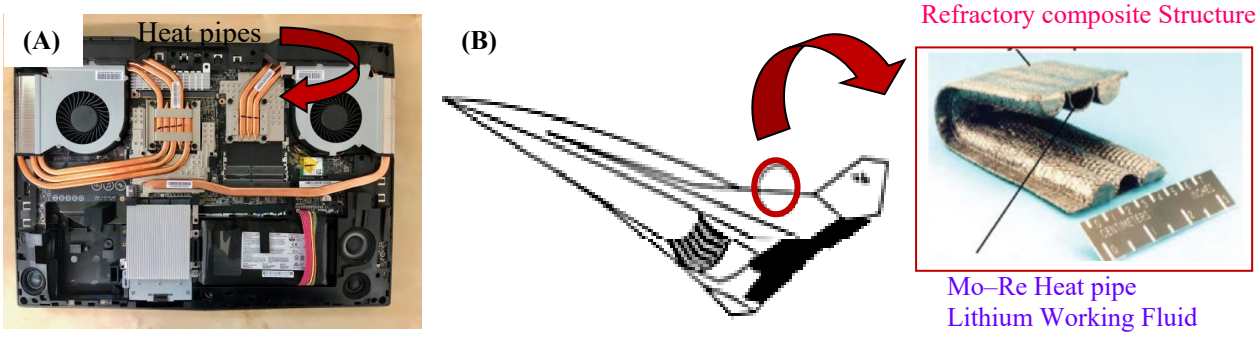

Figure 2. In (A) Heat pipes applied to cooling on notebooks (Zohuri et al., 2016) and in (B) C-shaped heat pipe for thermal protection in hypersonic vehicles (Rong et al, 2016).

NASA is developing the KILOPOWER system, shown in Fig. 3. The KILOPOWER operates in the 1 to 10 kW range. It uses eight alkali metal (Sodium) heat pipes to supply heat to 8 Stirling convertors to produce electricity. And it uses titanium water heat pipes to remove the waste heat and transport it to the radiators, to be rejected to space (Gibson et al, 2017). The sodium heat pipe has an external diameter of 12.7 mm and carries 380 W. The titanium heat pipe has an external diameter of 15.9 mm and dissipates 125 W.

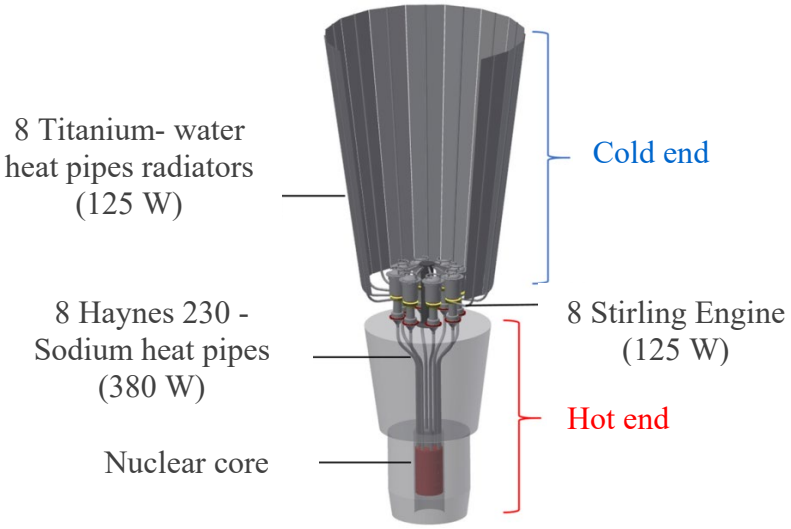

Figure 3. Kilopower nuclear fission system and the thermal management system – Adapted (Gibson et al, 2017).

The TERRA project conducted by the Institute for Advanced Studies (IEAv) researches and develops technologies for power generation in remote and inhospitable places, such as space. One of the technologies is Stirling engines, which are thermal machines that convert heat into electrical energy. Nuclear fission energy is the most suitable for harsh environments. However, to carry the heat from this nuclear source to the Stirling engine, one uses a heat pipe device to perform this heat transport.

The IEAv developed a Stirling engine (Santos et al., 2020) and screen copper-water heat pipes (Euphrásio, 2019). IEAv intends to perform a test in the future using heat pipes to transport heat from a nuclear source to the Stirling engine for electricity generation, as shown in Fig. 4. Before that, it is necessary to have a better fill of some parameters, such as, for instance, the gravity influence on the performance of the pipes. Thus, the objective of this work is to experimentally evaluate the relationship of the angle of inclination (gravity) influence of a heat pipe on the thermal performance of two copper screen-water heat pipes with different porosities (30 and 100 mesh). This analysis evaluates the best operating regime of the pipe for coupling to the engine.

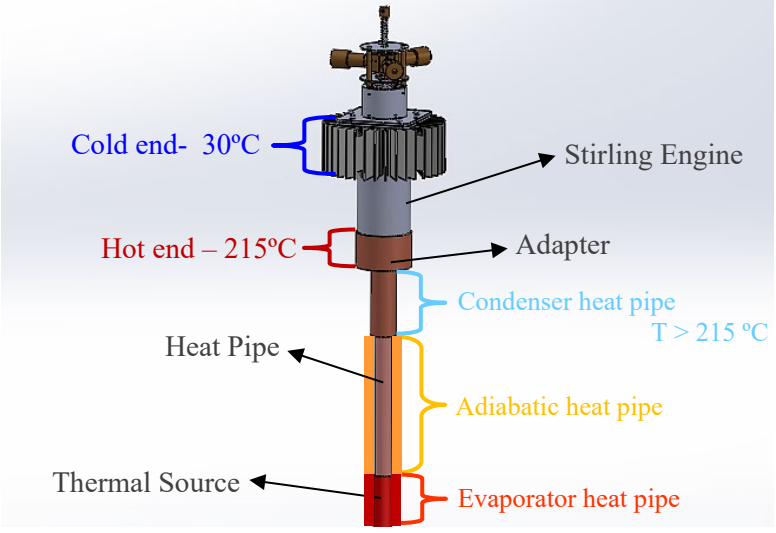

Figure 4. Schematic drawing of the assembly: heat pipe + Stirling engine (Santos et al., 2020).

Previous work developed by Santos et al (2020) showed that the condenser temperature must reach at least 215ºC. This value is sufficient to conduct heat to the adapter and activate the Stirling engine. In this work, the pipe has the function of transporting and not dissipating heat. Therefore, a minimum temperature difference between the evaporator and the condenser is required.

2. METHODOLOGY

2.1. Characteristics of the 100 and 30 mesh copper heat pipe

The heat pipes shown in Fig. 5 were developed by Euphrásio (2019) at IEAv. It is composed of a copper envelope, water as the working fluid, and a brass screen-capillary structure (30 and 100 mesh).

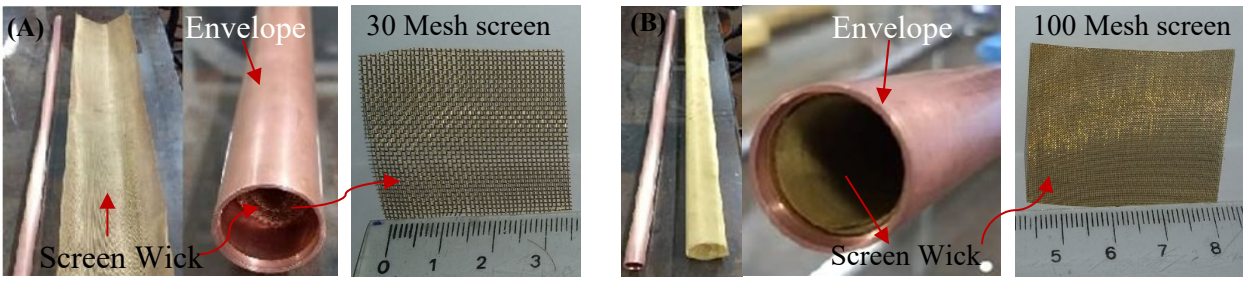

Figure 5. Photo of the heat pipe components: In (A) 30 mesh and (B) 100 mesh.

The dimensions specifications of those heat pipes are presented in Tab.1.

Table 1. Dimensions of Screen heat pipes existing in the IEAv.

External diameter	Inner diameter	Total length	Evaporator Length	Condenser Length	Fluid volume filled
0.0256 m	0.0226 m	0.960 m	0.200 m	0.200 m	46,5 mL

The adiabatic region of the pipes was isolated with an alumina ceramic fiber blanket (thickness of 25 mm and thermal conductivity of 0.071 W/(m K)). The condenser region was isolated with aluminum foil to avoid loss of heat. The evaporator region in all experiments was heated using a thermal heating belt (220 V) with a power controller. In addition, the belt was isolated by a ceramic fiber blanket.

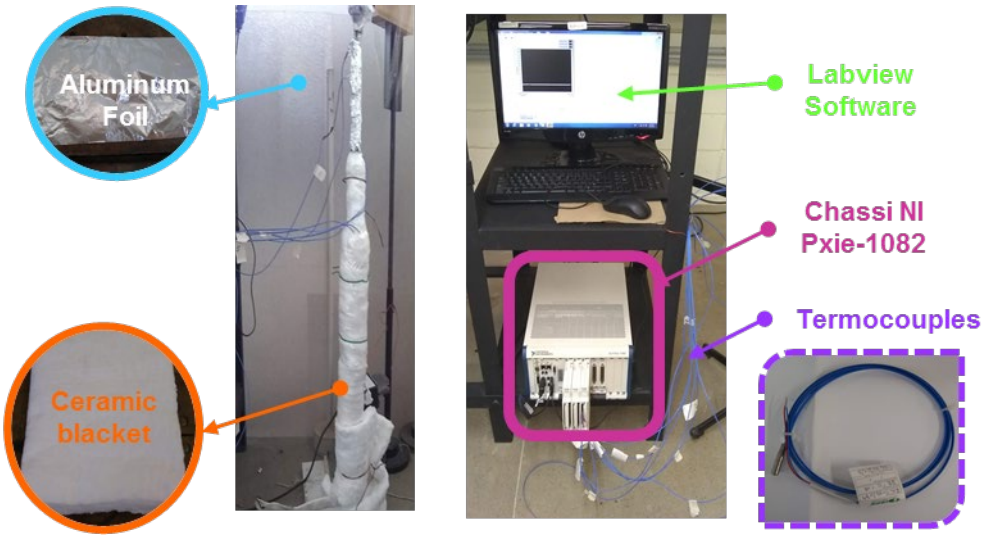

Figure 6. In (A) Heat pipe assembly and (B) Data collection system: thermocouples coupled to the Chassis.

2.2. Experimental Apparatus

Seven T-IOPE thermocouples were calibrated for temperature range between 20 ºC and 300 ºC (Instrument uncertainty ± 0.92 ºC and coverage factor, k = 2). The T thermocouples were connected to the predetermined pipe positions shown in Fig. 7. The NI PXIe-1082 chassis shown in Fig. 6 (B) was used for temperature data collection. The software used to collect pipe temperatures was developed in Labview. The heat pipes were subjected to varying angles of inclination in relation to the surface (0º, 30º, 45º, 60º, and 90º), as shown in Fig. 7 (B).

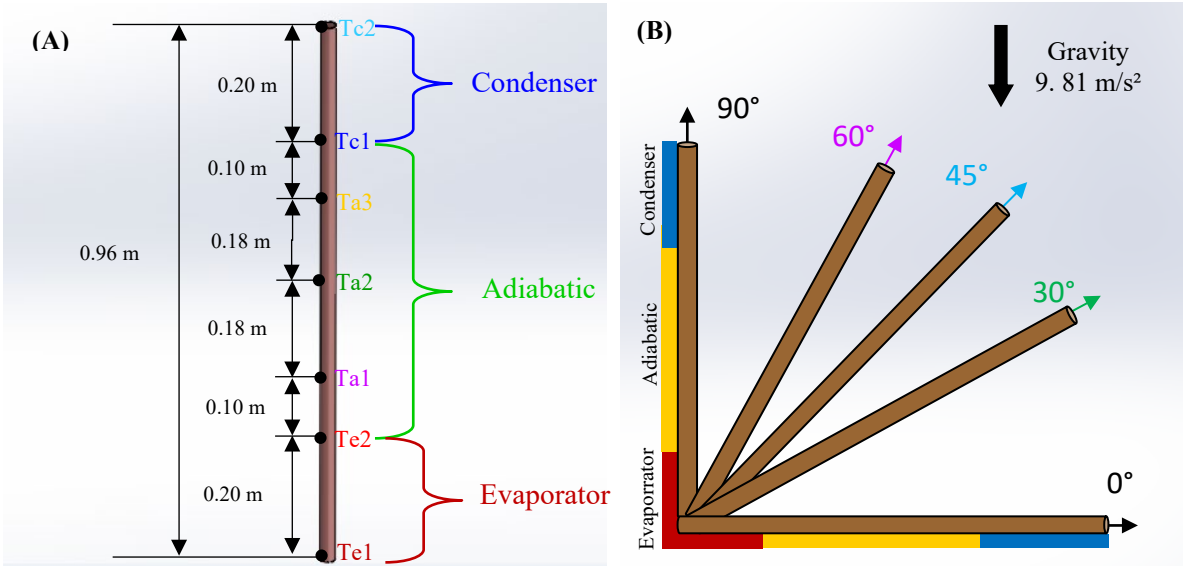

Figure 7. In (A) Drawing of the positions of the thermocouples in the heat pipe and in (B) Drawing of the angle of the pipe inclination in relation to the horizontal (0º, 30º, 45°, 60° and 90°).

The heat was applied gradually to the pipe evaporator. The electrical currents tested were: 0.833 A, 0.972 A, 1.11 A, and 1.25 A. At each current, the pipe was expected to enter a steady state. The pipe temperatures set were collected from the moment of thermal ribbon turn on until a steady-state reach. With the temperatures collected, calculations were performed to characterize its thermal behavior. An Excel program was developed using the equations by (Reay et al, 2006) and (Zohuri, 2016). The heat flow rate q (W) is obtained by Eq. (1).

$$q = \frac{\Delta T}{R} = \frac{T_e - T_c}{R} \tag{1}$$

Where: T_e is the evaporator wall temperature T_c is the condenser wall temperature and R is the global thermal resistance (ºC/W) which considers the internal and external resistances of the heat pipe obtained by Eq. (2).

$$R = \frac{1}{h_e \cdot A_e} + \left(\frac{\left[\ln\left(\frac{D_e}{Di}\right) + \ln\left(\frac{D_i}{Dv}\right)\right]}{\pi \cdot \left[l_e \cdot k_{copper} + l_e \cdot k_{eff} + l_c \cdot k_{eff} + l_c \cdot k_{cooper}\right]} \right) + \frac{1}{h_c \cdot A_c} \tag{2}$$

Where: D_i is the inner diameter (m), D_e is the external diameter (m), D_v is the vapor diameter (m), L_e is the evaporator length (m), L_c is the condenser length (m), A_e is the evaporator lateral area (m²), A_c is the condenser lateral area (m²), h_e is the evaporator external convection heat transfer coefficient (W/m² K), h_c is the condenser external convection heat transfer coefficient (W/m² K), k_{cooper} is the thermal conductivity of envelope material (W/m K) and k_{eff} is the effective thermal conductivity (W/m K) obtained by Eq. (3).

$$k_{eff} = \frac{k_l \cdot [(k_l + k_w) - (1 - \varepsilon)(k_l - k_w)]}{[(k_l + k_w) + (1 - \varepsilon)(k_l - k_w)]} \tag{3}$$

k_l is the thermal conductivity of the working fluid (W/m K), k_w is the thermal conductivity of wick material (W/m K) and ε is the mesh porosity. The operational limits: viscous, sonic, boiling, capillary were obtained by Eq. (4-7).

$$q_{viscous} = \frac{{d_v}^2 \cdot h_{lv} \cdot \rho_v \cdot p_v}{64 \cdot \mu_v \cdot \{[(l_e + l_c)/2] + l_a\}} \tag{4}$$

$$q_{sonic} = 0{,}474 \cdot h_{lv} \cdot A_v \cdot \sqrt{\rho_v \cdot p_v} \tag{5}$$

$$q_{boiling} = \left(\frac{2\pi \cdot l_e \cdot k_{eff} \cdot T_v}{h_{lv} \cdot \rho_v \cdot \ln\left(\frac{D_i}{D_v}\right)} \right) \cdot \left(\frac{2\sigma}{2{,}54 \times 10^{-6}} - P_c \right) \quad (6)$$

$$q_{capillary} = \frac{\sigma \cdot \rho_l \cdot h_{lv}}{\mu_l} \cdot \frac{K \cdot A_w}{[(l_e + l_c)/2] + l_a} \cdot \left(\frac{2}{r_{eff}} - \frac{\rho_l \cdot g \cdot (l_e + l_a + l_c) \cdot (\cos \cdot \psi)}{\sigma_l} \right) \quad (7)$$

Where T_v is the vapor temperature (K), A_v is the cross sectional area of vapor diameter (m²), ρ_v is the vapor density (Kg/m³), ρ_l is the liquid density (Kg/m³), p_v is the vapor pressure (Pa), P_c is the capillary pressure (Pa), μ_v is the vapor dynamic viscosity (Kg/m s), μ_l is the liquid dynamic viscosity (Kg/m s), h_{lv} is the latent heat of vaporization (J/kg), σ is the superficial tension (N/m), r_{eff} is the effective capillary radius, K is the wick permeability, ψ is the inclination angle of heat pipe and g is the gravity (m/s²).

3. RESULTS AND DISCUSSIONS

Figures 8 and 9 show the temperature distribution graphs at angles: 0º, 30º, 45º, 60º, and 90º. All graphs show that the greater the electrical current applied to the evaporator (consequently electrical power), the greater the temperature differential in the heat pipe.

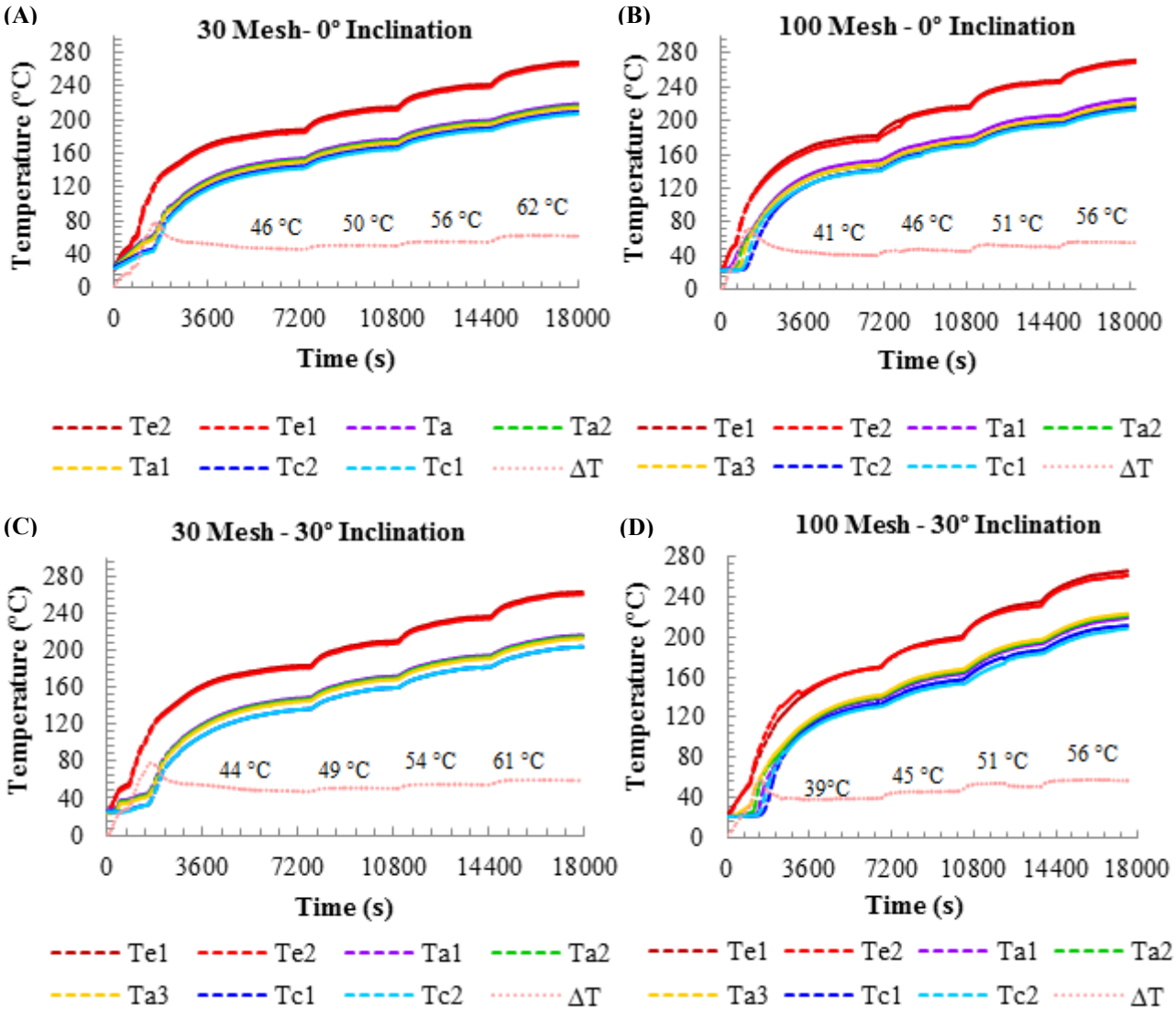

Figure 8. Comparison of the temperature distribution in the 30 and 100 mesh heat pipes with varying angle inclination: In (A) and (B) 0° inclination, in (C) and (D) 30° inclination.

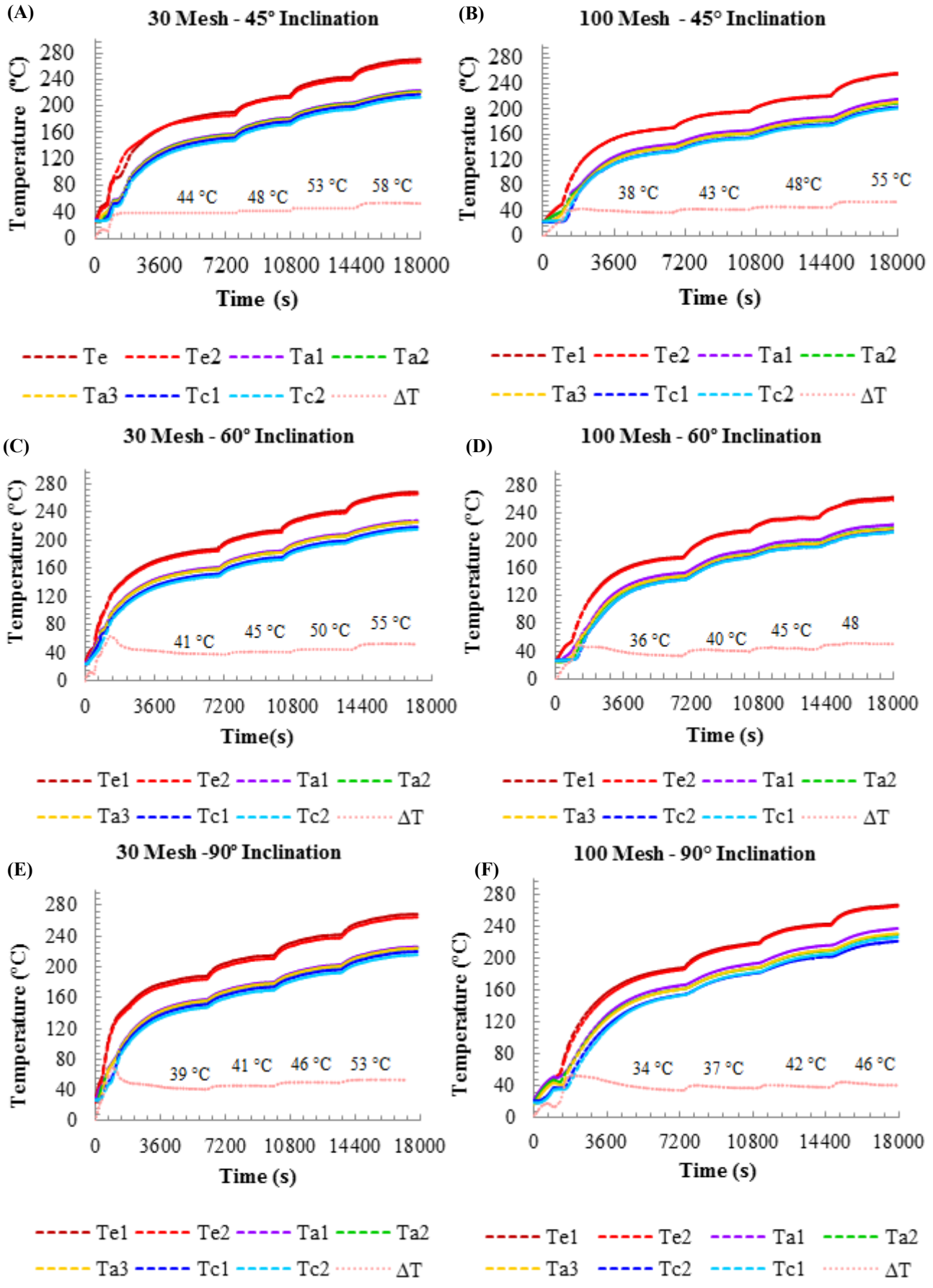

Figure 9. Comparison of the temperature distribution in the 30 and 100 mesh heat pipes with varying angle inclination: In (A) and (B) 45° inclination, in (C) and (D) 60° inclination, in (E) and (F) 90° inclination.

Figure 10 shows the temperature difference graphs between the evaporator and condenser. Both heat pipes reached at least 215°C in the condenser on all slopes. This temperature is sufficient to activate the studied Stirling engine. However, the temperature differential (ΔT) of the 100 mesh heat pipe is less than 30 mesh. In angulations where gravity is favorable (90º and 60º), the ΔT is less than in positions where gravity is unfavorable. At 0° and 30°, the temperature differential is higher than at angles above 45°. Above 45º, gravity is the driving force to transport the condensed liquid. At 30°, the liquid return occurs by the sum of the capillary action and gravity. At 0º angle, the condensed liquid is returned to the evaporator using a wick structure by capillary action (in this case, screen).

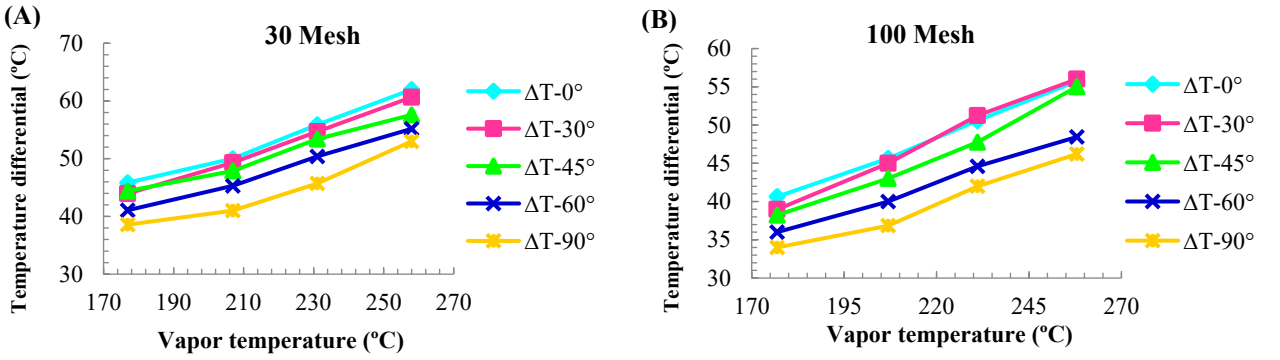

Figure 10. Comparison of the temperature difference of the 30 and 100 mesh heat pipes with varying inclination.

Both pipes have the same geometry, dimensions, working fluid (water), and the same material (copper). Thus, the difference in ΔT occurs exclusively due to the difference in porosity of the meshes. Porosity influences the permeability, capillary pressure, and effective thermal conductivity of the heat pipe. The lower the porosity, the greater the thermal conductivity. The high thermal conductivity results in a small temperature drop through the capillary structure. The porosity of the 30 mesh is 73%, and the 100 mesh is 67%. Therefore, the thermal conductivity of 100 mesh is greater than that of mesh 30, as can be seen in Fig. 11 (A). The higher conductivity of the 100-mesh allows for a lower temperature differential. It is interesting to note that the effective conductivity decreases significantly after 150ºC due to the decrease in the conductivity of the water. The porosity of the mesh influences the capillary pressure, responsible for transporting the liquid. Figure 11 (B) shows the comparison of the capillary pressure of the heat pipes. The 100 mesh screen has less porosity than the 30 mesh. Therefore, it has a higher capillary pressure value, that is, a higher transport capacity value.

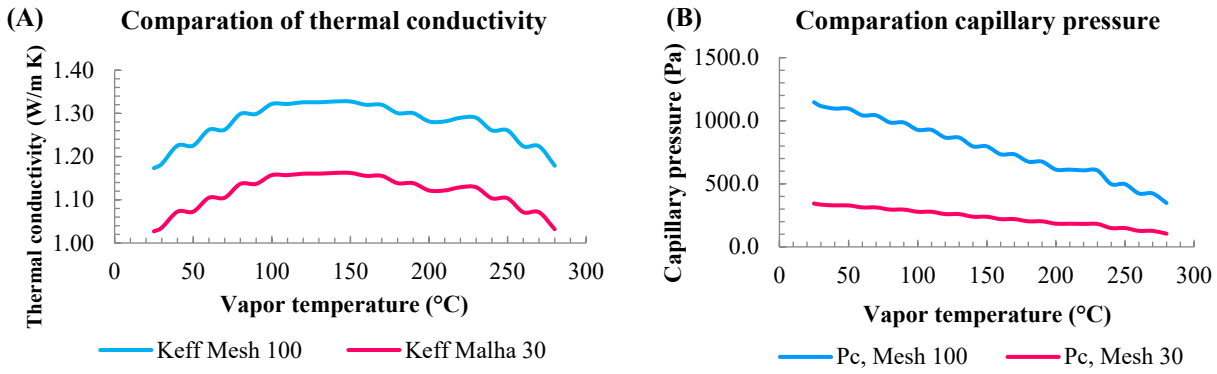

Figure 11. Comparison of thermal conductivity (A) and capillary pressure (B) between heat pipes (30 and 100 mesh).

Figures 12 (A) and (B) shows the thermal resistances according to the inclination angle and vapor temperature. In general, resistance decreases with increasing temperature. The slope variation has little impact on the value of thermal resistances. The thermal resistances of the 30 mesh heat pipe have higher values than the 100 mesh at all slopes. The resistances have values on the order of 1. The high value is due to the high external resistances. To decrease this value, it is necessary to increase the convection of the environment or increase the surface area of the pipe. However, even so, these heat pipes serve the purpose of this work. In addition, the pipes have less resistance than a hollow pipe of the same dimension, which is in the order of 10^2 according to Reay et al (2006). Figures 12 (C) and (D) show the thermal power versus vapor temperature. Note that power increases with the increase in the vapor temperature. On the other hand, it gradually decreases as the angle of inclination increases. Furthermore, the thermal power of the 100 mesh heat pipe is greater than 30 mesh due to the lower thermal resistance on all slopes.

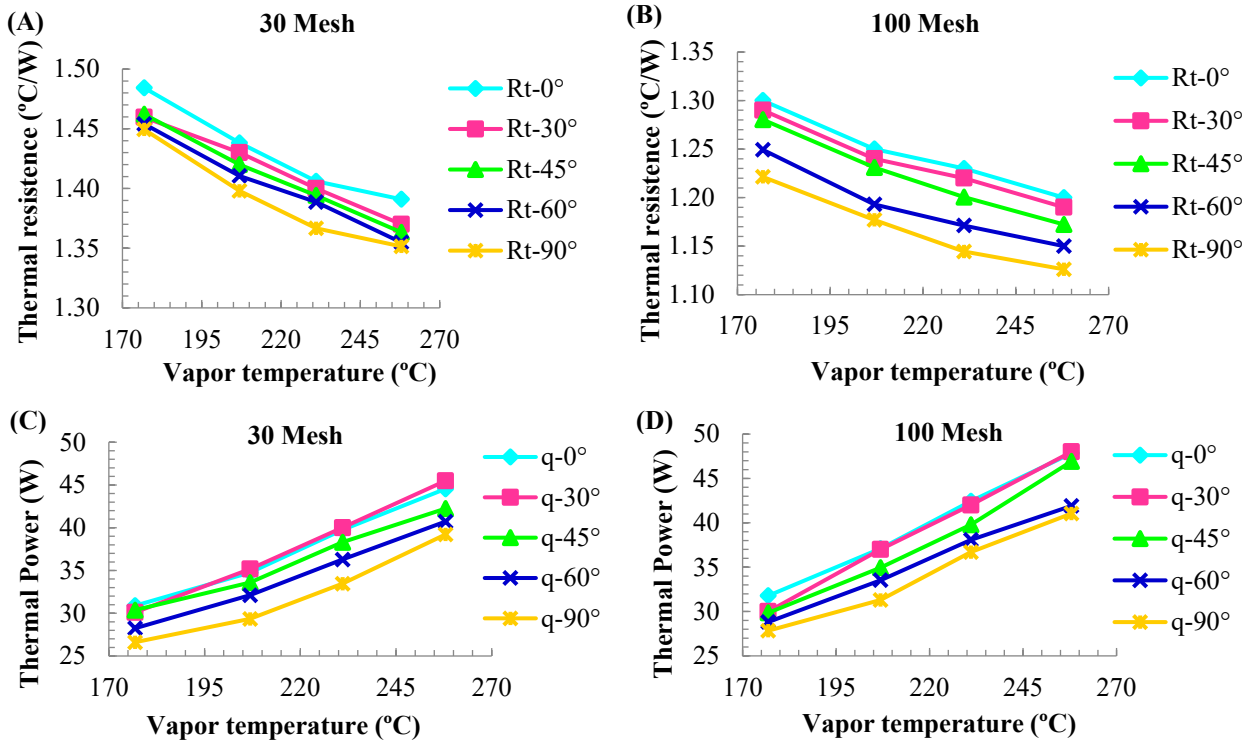

Figure 12. Comparison of the thermal resistance (A-B) and the thermal power (C-D) of the 30 and 100 mesh heat pipes.

Heat pipes developed by NASA (Gibson et al, 2017) made of titanium and water as a working fluid carry 125 W. In comparison, the copper water heat pipe used in this work carries an average of 45 W. This value is good considering the less robust materials used. Table 2 shows the pressure drops as a function of the inclination angle. The condition for a heat pipe to work in the 0° position is that the pipe's maximum capillary pressure (*Pc*) is greater than the sum of the other pressure drops ($\sum p$). When the capillary pressure is less than the sum of the pressure drops, it means that the heat pipe does not work by the action of the capillary force, but by the action of the gravitational force. In both pipes, in the 0° position, the capillary pressure is greater than the pressure drops, that is, the pipe works by capillary action.

Table 2- Pressure drops (Pa) in the temperature range of 265 ºC in heat pipes.

Angle	*30 Mesh*					*100 Mesh*				
	Pc	**Δ*pvl***	**Δ*p*+**	**Δ*p*|**	**∑*p***	***Pc***	**Δ*pvl***	**Δ*p*+**	**Δ*p*|**	**∑*p***
0º	183.7	5.8	157.2	0.0	163.0	606.3	223.1	173.9	0.0	400.0
30º	157.52	5.8	132.3	3957.28	4095.4	560.5	236.7	155.1	4073.1	4465.0
45º	128.6	5.4	108.0	5596.4	5709.9	433.2	226.2	126.6	5760.2	6113.0
60°	90.9	5.2	76.3	6854.2	6935.8	306.3	202.0	89.5	7054.8	7346.4
90º	0.0	5.0	0.0	7914.5	7919.6	0.0	173.5	0.0	7914.5	8088.0

Pc is the maximum pressure difference produced by the capillary effect of the screen mesh (Pa), **Δ*pvl*** - Sum of liquid and vapor pressure drop (Pa), **Δ*p*+** is the radial hydrostatic pressure drop (Pa), **Δ*p*\|** is the axial hydrostatic pressure drop (Pa) and **∑*p*** is sum of the pressure drops (Pa) that corresponds to the sum of the Δpvl, Δp+ and Δp|.

Note that even at 0° gravity acts on the radial hydrostatic pressure. In the other angulations (30°, 45°, 60°, and 90°), capillary pressure is less than the sum of the pressure drops. Thus, the return of the fluid occurs predominantly by the aid of gravity and not by capillarity. In addition, it is observed that 100 mesh heat pipe has greater capillary pressure than 30 mesh heat pipe. Therefore, it presents better heat transport in the absence of gravity. Table 3 shows the operating limits of the pipes in the same vapor temperature range (265ºC) and at different angles. In both heat pipes, the lowest operating limits are the boiling and entrainment limits. The maximum power transferred by the heat pipe (Project) is away from the operational limits. Thus, in these conditions of tests carried out, heat pipes do not reach any operating limit. Regardless of the angle, the pipe has very close operating limits because the calculation considers only vapor temperature. Therefore, in the same temperature range (265ºC), operating limits have similar values. In general, the operating limits of 100 mesh are higher than 30 mesh. It occurs due to the greater vapor diameter of 100 mesh (due to the lesser thickness of 100 mesh), so it can carry more heat.

Table 3- Operational limits of the heat pipes in the temperature range of 265 ºC.

	30 Mesh					*100 Mesh*				
	0°	**30°**	**45°**	**60º**	**90°**	**0°**	**30°**	**45°**	**60º**	**90°**
Capillary (W)	202.5	*	*	*	*	91.46	*	*	*	*
Entrainment (W)	3048.9	2883.7	2883.7	2883.7	2883.7	7234.4	7649.2	7649.1	7649.1	7234.5
Viscous $x10^{10}$ **(W)**	5.1	5.23	5.3	5.2	5.2	9.5	7.93	7.9	7.9	9.5
Sonic $x10^{4}$ **(W)**	7.00	6.61	6.61	6.62	6.61	8.58	8.95	8.96	8.93	8.56
Boiling (W)	1120.1	1212	1190.5	1200.1	1190.3	3930.1	3695.0	3720.2	3700.1	3980.3
Project (W)	44.5	45.5	42.2	40.7	39.2	47.8	53.2	46.9	41.9	41.0

*Not applicable.

4. CONCLUSIONS

This paper presented experimental research of the 100 and 30 mesh heat pipes existing at IEAv for application in the transport of heat from a thermal source to the hot tip of Stirling. To activate the Stirling engine, the condenser temperature must be at least 215ºC. The tests were carried out in the temperature range of 25º C to 270º C at different angles, and the condenser reached the required temperatures. The 100 mesh heat pipe has less porosity, permeability, and greater thermal conductivity than mesh 30. The higher value of thermal conductivity results in a lower temperature drop, as evidenced in the experiments. The 100 mesh pipe had a lower temperature gradient, lower resistance, and higher power than the 30 mesh pipe at all positions. Therefore, the 100-mesh pipe presents greater efficiency, that is, a greater amount of heat transferred in a lower temperature gradient.

The variation in the angle of inclination causes little significant difference in the performance of the heat pipes. In positions where gravity is favorable (90° and 60°), a lower temperature differential was observed than in positions where gravity does not act (0°) or acts little (30°). In positions where gravity is favorable, hydrostatic pressures are higher than capillary pressure, indicating that gravity is the predominant driving force. While at the 0° position the capillary pressure is greater than the hydrostatic pressure forces, indicating that the pipe works by capillary force. The maximum power transferred through the pipe is far from the operational limits. Thus, in these conditions of tests carried out, heat pipes do not reach any operational limit. Finally, the 100 mesh pipe has better properties. So, with this paper, it is possible to understand the operation of the pipes at the activation temperature of the Stirling and select the best heat pipe (100 mesh) and position (90º) for future experiments with the complete set.

5. ACKNOWLEDGEMENTS

This study was financed in part by the Coordenação de Aperfeiçoamento de Pessoal de Nível Superior – Brasil (CAPES) and the TERRA Project - Finance Code 001. Acknowledgments are provided to the IEAv for the use of the Laboratories and Felipe Euphrásio for the use of his heat pipe developed on his Master Program.

6. REFERENCES

Euphrásio P., F., 2019. “Desenvolvimento, construção e análise de funcionamento de tubos de calor”. Dissertação de mestrado em Ciências e Tecnologias Espaciais, Instituto Tecnológico de Aeronáutica, São José dos Campos, Brasil.

Gibson, M., Oleson, S.R., Poston, D., and Mcclure, P.R., 2017. "NASA's Kilopower Reactor Development and the Path to Higher Power Missions". In IEEE Aerospace Conference. Big Sky, United States.

Nemec, P., 2016. “Gravity in Heat Pipe Technology”. In book: Gravity - Geoscience Applications, Industrial Technology and Quantum Aspect. eBook (PDF) ISBN: 978-953-51-4059-7.

Reay, D. A.; Kew, P. A., 2006. Heat pipes: theory, design and applications. Elsevier's Science & Technology, Oxford, 5th edition.

Rong, Y., Wei, Y., Duan, D., and Zhan, R., 2016.“Heat-balance Thermal Protection with Heat Pipes for Hypersonic Vehicle.” In the International Seminar on Applied Physics, Optoelectronics and Photonics. MATEC Web of Conferences.

Santos, A. C., Guimarães, L. N. F., Leite, V. S. F. O. and Theodoro, R., 2020. “Characterization of a coupled copper-water heat pipe with a Free Piston Stirling Engine”. In Brazilian Congress of Thermal Sciences and Engineering - ENCIT. Online conference.

Zohuri, B., 2016. “Heat Pipe Design and Technology”. Modern Applications for practical thermal management. Springer Publishing company, New York, 2nd edition.

RESPONSIBILITY NOTICE

The authors are the only responsible for the printed material included in this paper.